A Pretargeted Imaging Strategy for EGFR Positive Colorectal Carcinoma via the Modulation of Tz-radioligand Pharmacokinetics

Lin Qiu
Zhongshan Hospital Fudan University

Hui Tan
Zhongshan Hospital Fudan University

Qingyu Lin
Zhongshan Hospital Fudan University

Zhan Si
Zhongshan Hospital Fudan University

Jun Zhou
Zhongshan Hospital Fudan University

Tingting Wang
Zhongshan Hospital Fudan University

Dengfeng Cheng
Zhongshan Hospital Fudan University

Hongcheng Shi
Fudan University

Original research

Keywords: Colorectal cancer, EGFR, Cetuximab, Pretargeted imaging, Click chemistry

Abstract

Objective: Previously, we successfully developed a pretargeted imaging strategy (Atezolizumab-TCO/99mTc-HYNIC-PEG11-Tz), which is a powerful tool for evaluating Programmed Cell Death Ligand-1 (PD-L1) expression in xenograft mice tumor models. However, the surplus unclicked 99mTc-HYNIC-PEG11-Tz is cleared somewhat sluggishly through the intestines. This is certainly not an ideal situation for imaging for colorectal cancer (CRC). In order to shift the excretion of the Tz-radioligand to the renal system, we have sought to develop a novel Tz-radioligand by adding a polypeptide linker between HYNIC and PEG11.

Methods: Pretargeted molecular probes 99mTc-HYNIC-Polypeptide-PEG11-Tz and Cetuximab-TCO were synthesized. The stability of 99mTc-HYNIC-Polypeptide-PEG11-Tz was evaluated in vitro, and its blood pharmacokinetic test was performed in vivo. In vitro ligation reactivity of 99mTc-HYNIC-Polypeptide-PEG11-Tz towards Cetuximab-TCO was tested. The biodistribution and imaging of 99mTc-HYNIC-Polypeptide-PEG11-Tz was performed to observe the clear pathway of this novel Tz-radioligand. Pretargeted biodistribution of three different accumulation intervals was performed to determine the optimal pretargeted interval time. Comparison of pretargeted (Cetuximab-TCO 48 h/99mTc-HYNIC-PEG11-Tz 6 h) and (Cetuximab-TCO 48 h/99mTc-HYNIC-Polypeptide-PEG11-Tz 6 h) imagings was performed to show the effect of the two Tz-radioligands with different excretion pathway on tumor imaging.

Results: 99mTc-HYNIC-Polypeptide-PEG11-Tz showed favorable in vitro stability and rapid blood clearance in mice. SEC-HPLC revealed almost complete reaction between Cetuximab-TCO and 99mTc-HYNIC-Polypeptide-PEG11-Tz in vitro, with the 8:1 Tz-to-mAb reaction providing a conversion yield of 87.83 ± 3.27%. The biodistribution and imaging of 99mTc-HYNIC-Polypeptide-PEG11-Tz demonstrated that the Tz-radioligand was cleared through kidneys. After allowing 24 h, 48 h and 72 h for accumulation of Cetuximab-TCO in HCT116 tumor, pretargeted biodistribution revealed the tumor-to-blood ratio was 0.83 ± 0.13, 1.40 ± 0.31, and 1.15 ± 0.21, respectively. Both pretargeted (Cetuximab-TCO 48 h/99mTc-HYNIC-PEG11-Tz 6 h) and (Cetuximab-TCO 48 h/99mTc-HYNIC-Polypeptide-PEG11-Tz 6 h) imaging delineated the HCT116 tumor clearly. However, pretargeted imaging strategy using Cetuximab-TCO/99mTc-HYNIC-Polypeptide-PEG11-Tz could be used for diagnosing CRC since the surplus unclicked 99mTc-HYNIC-Polypeptide-PEG11-Tz is cleared through urinary system and produces low abdominal uptake background.

Conclusion: We developed a novel pretargeted imaging strategy (Cetuximab-TCO/99mTc-HYNIC-Polypeptide-PEG11-Tz) for imaging CRC since the surplus unclicked 99mTc-HYNIC-Polypeptide-PEG11-Tz produces low abdominal uptake background, which broadens the application scope of pretargeted imaging strategy.

1. Introduction

Colorectal cancer (CRC) is a common malignant tumor of the gastrointestinal tract with its morbidity ranking 3th among all malignant tumors and its mortality ranking 4th in the world, which poses a serious threat to human health [1]. In recent years, with the changes of lifestyle, the incidence of CRC has been increased year by year. Early diagnosis and treatment will greatly improve the prognosis of CRC, most of which could be cured in the early stage with a 5-year survival rate of 90%, while only 12.5% for advanced CRC [2]. Therefore, it is greatly significant for the diagnosis of CRC, especially for the early diagnosis, to research and develop the specific targeted molecular probe for CRC. At present, the clinical diagnosis for CRC mainly relies on endoscopy and endoscopy-guided biopsy, imaging methods such as computed tomography (CT), magnetic resonance imaging (MRI), and 2-deoxy-2-[^{18}F]fluoro-D-glucose (^{18}F-FDG) positron emission tomography/computed tomography (PET/CT). Invasive pathological biopsy guided by endoscopy is still the gold standard for clinical diagnosis of CRC. Common endoscopy mainly relies on morphological changes for the diagnosis of CRC, and it is easy to miss lesions with insignificant morphological changes, especially for early and micro lesions [3]. With the development of magnifying endoscopy, confocal laser endoscopy, and fluorescence endoscopy, endoscopic techniques could detect microscopic pathological changes and increase the diagnosis level of CRC. However, it is still difficult to detect surrounding tissue invasion and distant metastasis and achieve targeted imaging of CRC for these endoscopic methods. Anatomical imaging methods such as endoscopic ultrasonography, CT, or MRI have obvious advantages in the evaluation of surrounding tissue infiltration, lymph node and distant metastasis. But the imaging techniques are not specific for the diagnosis of CRC. As a functional imaging technology, ^{18}F-FDG PET/CT can reflect the tumor glucose metabolism. However, the most common positron radioactive tracer, ^{18}F-FDG, is still not a specific targeting molecular probe for CRC.

Currently, targeted molecular probes for CRC mainly include antibody [4-6], polypeptide [7, 8], and nanoparticle [9, 10] probes for epithelial growth factor receptor (EGFR) or vascular endothelial growth factor (VEGF). Antibody probes have exquisite affinity and selectivity for molecular targets such as EGFR or VEGF overexpressed by CRC. However, due to the slow pharmacokinetics, the use of antibodies as tracers requires labeling with isotopes with long half-lives (e.g., ^{111}In, ^{64}Cu, or ^{131}I), which significantly increases the radiation dose to non-target tissues. Polypeptide probes have several advantages over antibody probes including low molecular weight, reduced circulation time, easy access to target sites, and passivity to the immune system with little or no immunogenicity. However, the stability and affinity to target sites vary among different polypeptide tracers. Nanoparticle probes are equipped with different targeting units for different receptors, but this type of probe poses a potential threat of immunogenicity and renal toxicity.

EGFR has become a therapeutic target for CRC due to the close association of the EGFR expression with disease progression and metastasis [11]. The therapeutic antibody Cetuximab has been approved by FDA for treating CRC. As EGFR inhibitor, Cetuximab specifically targets the extracellular domain of the EGFR and block the intracellular tyrosine kinase activity. Moreover, molecular tracers using Cetuximab labeled with the long-lived radionuclides (such as ^{111}In, ^{89}Zr, ^{64}Cu, and ^{124}I) have been developed to detect the EGFR expression and evaluate the therapeutic response to EGFR-blocking [12-16]. However, extended

circulation time of radiolabeled antibodies creates prohibitively high radiation dose to healthy organs and low tumor/background imaging contrast. In this study, we will develop a novel pretargeted imaging strategy for evaluating EGFR expression of CRC.

Previously, we developed a pretargeted single photon emission computed tomography (SPECT) imaging strategy for evaluating immune checkpoint ligand PD-L1 expression in tumor based on bioorthogonal Diels-Alder click chemistry [17]. The molecular probe mainly includes two components: TCO-modified Atezolizumab (Atezolizumab-TCO) that could target PD-L1 and ^{99m}Tc labeled Tz-radioligand (^{99m}Tc-HYNIC-PEG$_{11}$-Tz). Pretargeted (Atezolizumab-TCO/^{99m}Tc-HYNIC-PEG$_{11}$-Tz) imaging involve following steps: (1) Atezolizumab-TCO was first injected into the bloodstream. (2) Atezolizumab-TCO was binded specifically to PD-L1 overexpressed by tumor and concomitantly was cleared from the blood slowly. (3) Then ^{99m}Tc-HYNIC-PEG$_{11}$-Tz was injected. (4) ^{99m}Tc-HYNIC-PEG$_{11}$-Tz was binded to pretargeted Atezolizumab-TCO via *in vivo* click ligation of the two components, followed by the rapid clearance of the excess Tz-radioligand. The pretargeted imaging strategy clearly delineated PD-L1 expressing H1975 human lung cancer xenografts with high imaging contrast and significantly reduced background radiation dose to nontarget organs. However, the surplus unclicked ^{99m}Tc-HYNIC-PEG$_{11}$-Tz is cleared somewhat sluggishly through the intestines. This is, of course, not an ideal situation for imaging abdominal tumor, especially for CRC. Therefore, we will further try to develop a novel Tz-radioligand with more favorable pharmacokinetic profile.

We will add a polypeptide chain containing hydrophilic amino acids between the HYNIC and Tz to shift the excretion of the Tz-derivative to the renal system, thereby reducing abdominal uptake background and facilitating imaging abdominal tumors. Technetium (^{99m}Tc) is the most widely used radionuclide for diagnosis in SPECT imaging, which is easily obtained from ^{99}Mo/^{99m}Tc generator and presents a appropriate half-life (6.02 h) and electron emission energy (140 keV). Thus, ^{99m}Tc was still chosen as the radionuclide in the study. Ultimately, we developed another pretargeted imaging strategy based on the combination of Cetuximab-TCO and ^{99m}Tc-HYNIC-Polypeptide-PEG$_{11}$-Tz for EGFR expression of CRC due to the renal excretion of the novel Tz-radioligand, which further broaden the application scope of pretarged imaging strategy.

2. Materials And Methods

2.1 Reagents and materials

All reagents and solvents were obtained from commercial sources (Sigma-Aldrich, Peprotech, Merda, Thermo, BD Bioscience, Invitrogen, Millipore, Nest, Hyclone, and Corning) and used as received without further purification. Cetuximab solutions were obtained from Selleck Chemicals. Amine-reactive TCO-NHS was purchased from Click Chemistry Tools. 3-(4-Benzylamino)-1,2,4,5-tetrazine (Tz) bearing an amine-reactive linker and O-(2-aminoethyl)-O'-[2-(boc-amino)ethyl]-decaethylene glycol (NH$_2$-PEG$_{11}$-NHBoc) were

purchased from Xi'an KaiXin Biological. Na[^{99m}Tc]TcO$_4$ was purchased from Shanghai Atom Kexing Pharmaceutical Co., Ltd. All solvents used for HPLC analysis within this project were HPLC grade.

2.2 mAb-TCO modification and characterization

0.2 M NaHCO$_3$ was added to Cetuximab in PBS solution (817 µl, 12.12 mg/ml) to make the final buffer pH as 8.6. To this solution was added an appropriate volume of TCO-NHS in N,N-dimethylacetamide to make final protein concentration as 3.0 mg/ml, N,N-dimethylacetamide content as 10%, and TCO/mAb reaction stoichiometry as 35:1. The resulting solution was incubated with gentle shaking for 3 h at room temperature in dark. Subsequently, a 40 KD Zeba™ spin desalting column (Thermo Fisher Scientific) was used for the buffer exchange and purification of the final product. Aggregation and purity of the product were determined with SEC-HPLC. Protein concentration of this product was determined by spectrophotometer at the 280 nm absorbance. The final product was stored in PBS (pH = 7.4).

3.2 µl N,N-Dimethylformamide (DMF) and 2.8 µl 8 mg/ml HYNIC-Polypeptide-PEG$_{11}$-Tz solution in DMF were added to 24 µl of the product obtained in above step, resulting in a total volume of 30 µl and a Tz/Cetuximab ration of 20. As a control group, 3.2 µl DMF and 2.8 µl 8 mg/ml HYNIC-Polypeptide-PEG$_{11}$-Tz solution in DMF were added to 24 µl PBS solution to make the total volume of the reaction solution to be 30 µl. The reaction solution was incubated with gentle shaking at 37 °C for 20 minutes in dark, and then the consumption of HYNIC-Polypeptide-PEG$_{11}$-Tz was determined with reversed-phase high performance liquid chromatography (RP-HPLC) to calculate the average number of TCO conjugated to each Cetuximab.

2.3 Synthesis of Tz derivatives, radiolabelling with ^{99m}Tc and *in vitro* stability assay

We designed the chemical structures of HYNIC-PEG$_{11}$-Tz and HYNIC-Polypeptide-PEG$_{11}$-Tz, as indicated in Figure 1. Detailed synthesis route procedures are described in our previous work [17] and supplementary material. HYNIC-PEG$_{11}$-Tz and HYNIC-Polypeptide-PEG$_{11}$-Tz was labeled with ^{99m}Tc using tricine as coligand. Briefly, 185 MBq of Na[^{99m}Tc]TcO$_4$ (up to 100 µl) was added to a mixed solution containing 20 µg HYNIC-PEG$_{11}$-Tz or 40 µg HYNIC-Polypeptide-PEG$_{11}$-Tz, 200 µl of tricine solution in water (100 mg/ml), 1 µl of freshly prepared solution of SnCl$_2$ (1 mg/ml in 10^{-3} M HCl). The pH of the mixture was adjusted to 5.0 with HCl. After gently vortexing for a while, the reaction mixture was incubated at room temperature for 20 min. Radiochemical purity was determined by RP-HPLC using a gradient of 15:85 MeCN:H$_2$O (both with 0.1% TFA) to 45:55 MeCN:H$_2$O over 20 min. The procedures of *in vitro* stability assay of HYNIC-Polypeptide-PEG$_{11}$-Tz in NS, PBS or FBS refer to our previous work [17].

2.4 Distribution coefficient assay

10 µl of radiolabelled ^{99m}Tc-HYNIC-PEG$_{11}$-Tz or ^{9m}Tc-HYNIC-Polypeptide-PEG$_{11}$-Tz was placed in an Eppendorf tube containing 500 µl of n-octanol and 500 µl of PBS (pH = 7.4) solutions. The tube was vortexed vigorously for 1 min and then centrifuged at 12000 rpm for 5 minutes. The n-octanol/PBS (pH =

7.4) distribution coefficient was calculated in triplicate for each product. For each replicate, 10 µl solution was collected from both phases. Finally, the radioactivity of each fraction was measured in a γ-counter. The distribution coefficient was calculated as logD (logD = $\log_{10}$ n-octanol counts/aqueous phase counts).

2.5 *In vitro* cycloaddition reaction between Cetuximab-TCO and ^{99m}Tc-HYNIC-Polypeptide-PEG$_{11}$-Tz

With the pretargeted molecular probes ^{99m}Tc-HYNIC-Polypeptide-PEG$_{11}$-Tz and Cetuximab-TCO in hands, the reactivity of ^{99m}Tc-HYNIC-Polypeptide-PEG$_{11}$-Tz towards Cetuximab-TCO was first tested *in vitro* (n = 3). Typically, 100 µg Cetuximab-TCO was incubated with 8-fold molar equivalents of ^{99m}Tc-HYNIC-Polypeptide-PEG$_{11}$-Tz at 37 °C for 30 min. Then, 20 µl reaction solution was injected directly into SEC-HPLC. The fraction of cycloaddition reaction compound (^{99m}Tc-HYNIC-Polypeptide-PEG$_{11}$-Tz/TCO-Cetuximab) was determined by integrating the radioactive peak corresponding to the ligation compound.

2.6 Pretargeted cell immunoreactivity binding assay

HCT116 human CRC cells were obtained from Cell Bank of the Chinese Academy of Sciences. The cells were cultured in RPMI-1640 medium, which was supplemented with 10% fetal bovine serum and 1% penicillin-streptomycin. The cells were cultured at 37 °C in a humidified atmosphere with 5% CO_2. HCT116 cells were seeded in 24-well plate and grown to 80% confluence. Experimental group and control group cells were incubated for 2 h with Cetuximab-TCO (100 nM) and Cetuximab in 500 µl RPMI 1640 medium, respectively. Blocking group cells were pretreated by adding an excess of unmodified Cetuximab (100-fold) to the wells 2 h prior to incubation with Cetuximab-TCO. Then, the cells were washed with PBS three times and incubated for 30 min with ^{99m}Tc-HYNIC-Polypeptide-PEG$_{11}$-Tz (0.1 µg, 4.63 MBq/µg) in 200 µl PBS. After the incubation period, the cells were washed with PBS three times and then lysed with aqueous NaOH (2 M). The membrane-bound activity of each group was determined by measuring the radioactivity of lysed cells using a γ-counter.

2.7 *In vivo* pharmacokinetics, biodistribution and imaging of ^{99m}Tc-HYNIC-Polypeptide-PEG$_{11}$-Tz

The pharmacokinetics, biodistribution and SPECT imaging studies of ^{99m}Tc-HYNIC-Polypeptide-PEG$_{11}$-Tz alone were performed to investigate its pharmacokinetic profile, organ biodistriution and excretion pathway. Animal care and experimental procedures were approved by the Animals Ethics Committee of Zhongshan Hospital, Fudan University. For pharmacokinetics study, tumor-bearing mice (n = 3) were injected intravenously with ^{99m}Tc-HYNIC-Polypeptide-PEG$_{11}$-Tz and then blood from the tail vein was collected at serial time points (1, 3, 5, 7, 10, 15, 30 and 60 min). The blood samples were weighed and measured in a γ-counter along with standards to determine the percentage of the injected activity per gram of tissue mass (%IA/g).

For biodistribution and imaging studies, male athymic nude mice bearing subcutaneous HCT116 (right shoulder) xenografts were administered ^{99m}Tc-HYNIC-Polypeptide-PEG$_{11}$-Tz (16.65-18.50 MBq in 100 μl 0.9% sterile saline) via intravenous tail vein. Micro-SPECT/CT scans were conducted on the Nano SPECT/CT scanner (BioScan) at 30 min, 2 h, and 6 h post Tz-radioligand injection. Anesthesia and SPECT scan methods refer to our previous work [17]. Biodistribution experiments were performed at the same time point post Tz-radioligand injection with SPECT imaging. The mice were anesthetized with isoflurane and euthanized by cervical dislocation. Blood was withdrawn by heart puncture, and each organ and tissue of interest was harvested, blotted dry, and weighed. The radioactivity of each sample was measured using a γ-counter along with standards to determine the %IA/g for each sample of interest.

2.8 Pretargeted biodistribution study

Male athymic nude mice bearing subcutaneous HCT116 xenografts were administered 100 μg Cetuximab-TCO in 100 μl PBS via intravenous tail vein injection (The injected dose of 100 μg mAb-TCO was according to the published pretargeted tumor imaging studies [17-24]). In order to validate the optimal pretargeted interval time, three different accumulation intervals of 24 h, 48 h, and 72 h were performed in the pretargeted biodistribution study (n = 3). After three pretargeted accumulation periods, the same mice were then administered ^{99m}Tc-HYNIC-Polypeptide-PEG$_{11}$-Tz (16.65-18.50 MBq in 100 μl 0.9% sterile saline), also via tail vein injection. Six hours after the Tz-radioligand administration, the animals were anesthetized with isoflurane and blood was withdrawn by heart puncture (The time point of 6 h was chosen according to the results of our previous investigation [17]). Then the mice were euthanized by cervical dislocation, and tissue samples including tumor, heart, lung, liver, spleen, stomach, small intestine, large intestine, kidney, muscle, bone, skin, brain, thyroid, faces (in distal colon), and urine were harvested, blotted dry, and weighed. The radioactivity of all samples was measured in a γ-counter to determine the %IA/g.

2.9 Pretargeted biodistribution and imaging comparison

Nude mice bearing subcutaneous HCT116 xenografts were administered 100 μg Cetuximab-TCO via intravenous tail vein injection. After the appropriate accumulation interval (the highest tumor/blood ratio) of 48 h according to the results of pretargeted biodistribution study, the mice were then administered ^{99m}Tc-HYNIC-PEG$_{11}$-Tz or ^{99m}Tc-HYNIC-Polypeptide-PEG$_{11}$-Tz (16.65-18.50 MBq in 100 μl 0.9% sterile saline) intravenously. Biodistribution experiments and micro-SPECT/CT scans were conducted at 6 h post ^{99m}Tc-HYNIC-PEG$_{11}$-Tz or ^{99m}Tc-HYNIC-Polypeptide-PEG$_{11}$-Tz injection.

3. Results

3.1 Synthesis, characterization, radionuclide labeling, radiochemical purity, and *in vitro* reactivity of molecular probes

The reaction of Cetuximab modified by TCO-NHS ester was conducted in an alkaline environment (pH = 8.6) for 3 h. Then Cetuximab-TCO was purified by a 40 KD Zeba™ spin desalting column. The aggregation and purity of the product were 0.73% and 99.27% as shown by SEC-HPLC (Figure 2A). After the reaction of purified Cetuximab-TCO with 20-fold molar equivalents of HYNIC-Polypeptide-PEG$_{11}$-Tz was completed, the consumption of HYNIC-Polypeptide-PEG$_{11}$-Tz was used for calculating the average number of TCO conjugated to each Cetuximab. As shown in Figure 2B, the peak (Rt = 9.3 min) at red and blue curve was the ultraviolet (UV) absorption peak of unclicked HYNIC-Polypeptide-PEG$_{11}$-Tz at 280 nm in the control group and reaction group, respectively. The area under peak (Rt = 9.3 min) at the blue curve accounts for 59.5% of the corresponding red curve peak, indicating that HYNIC-Polypeptide-PEG$_{11}$-Tz consumed in reaction group accounted for 40.5%. Thus, the average reactive TCO moieties attached to each Cetuximab was 20 × 40.5% = 8.1.

The HYNIC-Polypeptide-PEG$_{11}$-Tz was synthesized mainly from a polypeptide chain (Gly-Arg-Glu-Arg-Glu-Lys) and three available building blocks: 3-(4-benzylamino)-1,2,4,5-tetrazine (Tz) bearing an amine-reactive linker, O-(2-aminoethyl)-O'-[2-(boc-amino)ethyl]-decaethylene glycol (NH$_2$-PEG$_{11}$-NHBoc), and 6-hydrazinonicotinyl (HYNIC) bearing a trifluoroacetyl protection group. The polypeptide chain was synthesized throughout Fmoc peptide solid phase synthesis method. Finally, the residue was purified by prep-HPLC (basic condition) to give HYNIC-Polypeptide-PEG$_{11}$-Tz as a red solid in a high purity (95.5%). HYNIC-Polypeptide-PEG$_{11}$-Tz was radiolabeled with ^{99m}Tc in a specific activity of 4.63 MBq/µg and a radiochemical purity of above 95% as confirmed by RP-HPLC.

The *in vitro* stability of ^{99m}Tc-HYNIC-Polypeptide-PEG$_{11}$-Tz was tested by incubation in NS, PBS, and FBS at 37 °C and subsequent HPLC analysis. As indicated in Figure 3, the Tz-radioligand remained relatively stable in the three media at early time point (generally above 85% radiochemical integrity in the three media after 2 h incubation). With time, however, decomposition of ^{99m}Tc-HYNIC-Polypeptide-PEG$_{11}$-Tz becomes apparent, especially in FBS (only 72.93 ± 2.51% and 63.10 ± 1.77% of the Tz-radioligand remained intact after 4 h and 8 h incubation, respectively). The *in vitro* stability of ^{99m}Tc-HYNIC-Polypeptide-PEG$_{11}$-Tz was similar to that of ^{99m}Tc-HYNIC-PEG$_{11}$-Tz [17].

The n-octanol/PBS (pH = 7.4) distribution coefficient assay of ^{99m}Tc-HYNIC-PEG$_{11}$-Tz and ^{99m}Tc-HYNIC-Polypeptide-PEG$_{11}$-Tz was performed to determine the effect of polypeptide modification on their hydrophilcity. ^{99m}Tc-HYNIC-Polypeptide-PEG$_{11}$-Tz showed a higher hydrophilic parameter with a logD of -4.64 ± 0.21, while a value of -3.75 ± 0.08 was observed for ^{99m}Tc-HYNIC-PEG$_{11}$-Tz. The incorporation of the hydrophilic polypeptide chain resulted in a more favorable distribution coefficient value, probably due to the charged and hydrophilic amino acid residue side chains present in the linker.

The *in vitro* reactivity of ^{99m}Tc-HYNIC-Polypeptide-PEG$_{11}$-Tz towards Cetuximab-TCO was tested in PBS at 37 °C for 30 min. Subsequently, a radio-SEC-HPLC analysis was performed. SEC-HPLC showed that the cycloaddition reaction between ^{99m}Tc-HYNIC-Polypeptide-PEG$_{11}$-Tz and Cetuximab-TCO proceeded near

completely, with the 8:1 Tz-to-mAb reaction stoichiometry providing an average yield of 87.83 ± 3.27% (Figure 4).

3.2 Pretargeted HCT116 cell immunoreactivity binding assay

Pretargeted cell immunoreactivity binding assay was performed using high EGFR-expressing HCT116 cell line. Pretargeted experimental group showed a high radioactivity retention in cells with an average counts per minute (CPM) value of 19,045 ± 557 (Figure 5). The control and blocking group cells showed a significantly lower activity with an average CPM value of 323 ± 52 and 2,326 ± 341, respectively ($P < 0.05$). The pretargeted cell immunoreactivity binding assay confirmed the specific binding of Cetuximab-TCO to HCT116 cells and verified preliminarily the feasibility of the molecular probes used for *in vivo* pretargeted imaging.

3.3 Molecular probe *in vivo* experiments

The pharmacokinetics, biodistribution and SPECT imaging experiments of ^{99m}Tc-HYNIC-Polypeptide-PEG$_{11}$-Tz alone were first performed to investigate its pharmacokinetic profile, tissue biodistribution and excretion pathway. The Tz-radioligand was cleared quickly from the circulation and distributed rapidly into various tissues and organs. The half-life ($t_{1/2}$) of blood distribution is 15.72 ± 1.83 min (Figure 6). The short blood $t_{1/2}$ ensures low radioactivity exposure to healthy organs and the background signal is relatively low when used for *in vivo* imaging. For biodistribution and imaging studies of ^{99m}Tc-HYNIC-Polypeptide-PEG$_{11}$-Tz alone, biodistribution experiment and Micro-SPECT/CT scans were conducted at 30 min, 2 h, and 6 h post the Tz-radioligand injection. Contrast to the hepatobiliary elimination pathway of ^{99m}Tc-HYNIC-PEG$_{11}$-Tz [17], ^{99m}Tc-HYNIC-Polypeptide-PEG$_{11}$-Tz was cleared completely through the urinary system, as indicated in Supplementary Table 1 and Figure 7. The radioactivity in the kidneys was 4.84 ± 1.89 %IA/g, 4.59 ± 0.82 %IA/g, and 2.98 ± 1.12 %IA/g at 30 min, 2 h, and 6 h post the Tz-radioligand injection, respectively. The Tz-radioligand was excreted quickly into bladder and the %IA/g of urine was 59.01 ± 36.71, 21.11 ± 23.80, and 4.21 ± 3.16 at 30 min, 2 h, and 6 h post the Tz-radioligand injection, respectively. The accumulation and retention of the radiotracer in liver, intestinal, and feces remained very low (< 0.3 %IA/g at various time points post the Tz-radioligand injection), indicating no hepatobiliary elimination pathway for the radioligand. The low uptake (< 0.2 %IA/g) in HCT116 tumor at all time points illustrated that the Tz-radioligand showed nonspecific binding to high EGFR-expressing HCT116 tumor. Critically, the accumulations in the thyroid and stomach were particularly low (< 0.3 %IA/g), suggesting the high *in vivo* stability of the Tz-radioligand. The SPECT imaging at each time point clearly visualized the biodistribution of ^{99m}Tc-HYNIC-Polypeptide-PEG$_{11}$-Tz in nude mice bearing subcutaneous HCT116 xenografts (Figure 8).

In order to validate the optimal pretargeted interval time, three different Cetuximab-TCO accumulation intervals of 24 h, 48 h, and 72 h were performed in the pretargeted biodistribution study (Supplementary Table 2 and Figure 9). Biodistribution experiments demonstrated the accumulation in kidneys and urine was relatively high with a %IA/g of more than 3.0 at each accumulation interval. After filtering through the

kidneys, the radiotracer concentrated in the bladder and finally excreted out of the body through urine. In addition to urinary system, high activity levels were observed in the tumor and blood (>1 %IA/g at each accumulation interval), suggesting a great incidence of *in vivo* click reactions in the blood in addition to ligations at the tumor. The tumor/blood ratio was 0.83 ± 0.13, 1.40 ± 0.31, and 1.15 ± 0.21, respectively after allowing 24 h, 48 h, and 72 h for accumulation of Cetuximab-TCO in HCT116 tumor. One-way analysis of variance revealed that the difference of tumor/blood ratio for 24 h, 48 h, and 72 h pretargeted interval was significant (F = 5.357, P < 0.05). Pair-wise comparisons of any two pretargeted intervals using LSD test revealed that, although tumor/blood ratio for 48 h and 72 h accumulation interval was not statistically different (P = 0.191), the difference of tumor/blood ratio for 24 h and 48 h accumulation interval was significant (P < 0.05). Thus, it becomes clear that 48 h represents a relatively more appropriate accumulation interval between the administration of mAb-TCO and the subsequent injection of Tz-radioligand. The accumulation and retention of the radiotracer in other organs including hypervascular lung, liver, and spleen remained generally very low, which suggested that the pretargeted strategy could efficiently improve the target/non-target ratio and significantly reduce background radiation dose to nontarget organs. Statistical analysis revealed that the radiotracer accumulation in HCT116 tumors was significantly higher than that in each organ/tissue (including heart, lung, liver, spleen, stomach, small intestine, large intestine, muscle, bone, skin, brain, and thyroid) for each pretargeted interval of 24 h, 48 h or 72 h (all P < 0.05).

According to the results of pretargeted biodistribution study, the most suitable accumulation interval (48 h) was chosen as the accumulation period of Cetuximab-TCO to compare the pretargeted Cetuximab-TCO/^{99m}Tc-HYNIC-PEG$_{11}$-Tz and Cetuximab-TCO/^{99m}Tc-HYNIC-Polypeptide-PEG$_{11}$-Tz biodistribution and SPECT imaging (Supplementary Table 3 and Figure 10). As ^{99m}Tc-HYNIC-PEG$_{11}$-Tz was cleared rapidly via the hepatobiliary system, the radioactivity in the liver, small intestine, and large intestine was relatively low with a %IA/g of 0.19 ± 0.11, 0.08 ± 0.13, and 0.08 ± 0.16, respectively at 6 h post ^{99m}Tc-HYNIC-PEG$_{11}$-Tz injection. The amount of activity in faces was relatively high (28.55 ± 24.66 %IA/g), suggesting that the surplus unclicked ^{99m}Tc-HYNIC-PEG$_{11}$-Tz is cleared rapidly through the intestines into the faces and remained in it. Additionally, a small amount of ^{99m}Tc-HYNIC-PEG$_{11}$-Tz was cleared through urinary system and the accumulation of urine was 1.20 ± 1.98 %IA/g after injecting the Tz-radioligand for 6 h. Pretargeted Cetuximab-TCO/^{99m}Tc-HYNIC-Polypeptide-PEG$_{11}$-Tz biodistribution demonstrated that the accumulation in kidneys and urine was relatively high with a %IA/g of 3.42 ± 0.61 and 21.98 ± 7.18, respectively. The uptake levels in liver, intestines, and faces were all less more 0.4 %IA/g, indicating that the surplus unclicked ^{99m}Tc-HYNIC-Polypeptide-PEG$_{11}$-Tz is cleared through urinary system. The tumor/blood ratio was 1.61 ± 0.12 and 1.40 ± 0.31, respectively for pretargeted Cetuximab-TCO/^{99m}Tc-HYNIC-PEG$_{11}$-Tz and Cetuximab-TCO/^{99m}Tc-HYNIC-Polypeptide-PEG$_{11}$-Tz biodistribution experiment. Both pretargeted Cetuximab-TCO/^{99m}Tc-HYNIC-PEG$_{11}$-Tz and Cetuximab-TCO/^{99m}Tc-HYNIC-Polypeptide-PEG$_{11}$-Tz imagings delineated the HCT116 tumor clearly and the imaging results were consistent with the results of biodistribution, as indicated in Figure 11. Pretargeted Cetuximab-TCO/^{99m}Tc-HYNIC-

Polypeptide-PEG$_{11}$-Tz imaging avoided the retention of the surplus unclicked Tz-radioligand in faces, which favors to specific targeting imaging for CRC.

4. Discussion

The pretargeted strategy (Atezolizumab-TCO/^{99m}Tc-HYNIC-PEG$_{11}$-Tz) that we previously developed could evaluate immune checkpoint ligand PD-L1 expression in tumor and simultaneously reduce the radiation dose to non-target organs [17]. However, the surplus unclicked ^{99m}Tc-HYNIC-PEG$_{11}$-Tz was cleared through hepatobiliary system and remained in faces for a long time, which is not favorable for imaging abdominal tumor, especially for CRC. In order to further broaden the application scope of pretarged imaging strategy, we added a polypeptide chain between the HYNIC and Tz to shift the excretion of the Tz-radioligand to the renal system, thereby facilitating imaging CRC.

In order to improve the hydrophilicity of previous ^{99m}Tc-HYNIC-PEG$_{11}$-Tz to facilitate renal excretion, we chose hydrophilic lysine, glutamate, and arginine in designing polypeptide sequence. Ultimately, the polypeptide sequence was determined as Gly-Arg-Glu-Arg-Glu-Lys and was synthesized successfully through the Fmoc-method. In order not to increase the steric resistance of click reaction between Cetuximab-TCO and Tz-radioligand, we added the polypeptide chain between HYNIC and PEG$_{11}$. Finally, the modified Tz-derivative structure was identified as HYNIC-Polypeptide-PEG$_{11}$-Tz. HYNIC-Polypeptide-PEG$_{11}$-Tz was labeled with radionuclide ^{99m}Tc in a similar manner to HYNIC-PEG$_{11}$-Tz. The radiochemical purity of final product ^{99m}Tc-HYNIC-Polypeptide-PEG$_{11}$-Tz was more than 95% and the specific activity was 4.625 MBq/µg. The stability of ^{99m}Tc-HYNIC-Polypeptide-PEG$_{11}$-Tz in NS, PBS and FBS was similar to that of ^{99m}Tc-HYNIC-PEG$_{11}$-Tz [17].

The urinary excretion of the polypeptide-modified ^{99m}Tc-HYNIC-Polypeptide-PEG$_{11}$-Tz is probably related to the increased hydrophilicity of the Tz-derivative results from hydrophilic amino acids and the presence of positive charge and lysine residue in the polypeptide chain. It is known that the Tz-scaffold part in the Tz-radioligands is hydrophobic. It is necessary to add hydrophilic structure to improve the hydrophilicity of the final Tz-derivative in the synthetic design of Tz-derivative. In the study conducted by Garcia et al. [18], ^{99m}Tc-HYNIC-PEG$_4$-Tz-Me was mainly cleared through the hepatobiliary system, and the relative absorption value of the liver and intestine was 9.91 ± 0.97 %IA/g and 23.35 ± 3.84 %IA/g, respectively at 1 h post the Tz-radioligand injection. The authors further added a polypeptide sequence between HYNIC and PEG$_4$ to increase the hydrophilicity of the Tz-radioligand to a logD of −1.05 ± 0.02. The newly synthesized Tz-radioligand was excreted mainly through kidneys. The relative absorption value of urine was 81.92 ± 5.06 %IA at 1 h post injection. In addition, Nichols et al. [25] and Devaraj et al. [26] successfully synthesized ^{68}Ga and ^{18}F-labeled Tz-coated polymer by introducing a well-established hydrophilic aminodextran backbone into the Tz-derivative, respectively. In our study, the n-octanol/PBS distribution coefficient of ^{99m}Tc-HYNIC-PEG$_{11}$-Tz and ^{99m}Tc-HYNIC-Polypeptide-PEG$_{11}$-Tz was -3.75 ±

0.08 and -4.64 ± 0.21, respectively. The modified ^{99m}Tc-HYNIC-Polypeptide-PEG$_{11}$-Tz showed a higher hydrophilic parameter compared to ^{99m}Tc-HYNIC-PEG$_{11}$-Tz.

It has been shown that the introduction of positive charge to radiopharmaceuticals can increase their renal clearance and retention [27-29]. Similarly, the introduction of positive charge in the Tz-radioligands increases clearance through the kidneys, whereas Tz derivatives with no charge were mainly excreted via the hepatobiliary system. In the study performed by Zeglis et al., as ^{64}Cu-NOTA-Tz is cleared somewhat sluggishly through the gastrointestinal pathway [22], the authors further created two novel Tz radioligands (^{64}Cu-NOTA-PEG$_7$-Tz and ^{64}Cu-SarAr-Tz) in order to improve their pharmacokinetic profiles [23]. For ^{64}Cu-SarAr-Tz, in addition to the change of the coordination environment from N_3O_3 to N_6, more importantly, the overall charge of the Tz-radioligand was shifted from −1 to +2. Finally, the newly synthesized ^{64}Cu-SarAr-Tz eliminates quickly and cleanly through the urinary tract [23]. In a pharmacokinetic profile study including 25 different Tz derivatives radiolabeled with either Al[^{18}F] or ^{68}Ga, Meyer et al. [30] observed that ^{68}Ga-NODA-Tz was excreted through renal pathway and Al[^{18}F]-NODA-Tz through hepatic and intestinal pathway. The authors suggested that the different excretion pathways of the two Tz-radioligands was resulted from the charge difference between ^{68}Ga-NODA-Tz (net charge: +1) and Al[^{18}F]-NODA-Tz (net charge: 0). In addition, the authors found that uncharged Al[^{18}F]-NOTA-lysine-Tz was excreted mainly through the liver and intestines, while charged Al[^{18}F]-NOTA-(lysine)$_2$-Tz (net charge: +1) and Al[^{18}F]-NOTA-(lysine)$_3$-Tz (net charge: +2) were excreted mainly through the kidneys [30]. Besides, it has been reported that renal uptake and excretion may be related to the presence of lysine residues in the molecular structure [31, 32].

After investigating three different Cetuximab-TCO accumulation internval of 24 h, 48 h, and 72 h, we found that the tumor/blood ratio was highest (48h: 1.40 ± 0.31 *vs.* 24 h: 0.83 ± 0.13 and 72 h: 1.15 ± 0.21) for allowing 48 h accumulation of Cetuximab-TCO, which represents a relatively more appropriate accumulation interval. After injecting Cetuximab-TCO for 24 h, the accumulation of the mAb-TCO at HCT116 tumor had not reached a saturation status due to its large molecular weight and poor tissue infiltration. Simultaneously, there existed a large of circulating Cetuximab-TCOs in the blood since most Cetuximab-TCOs had not been eliminated out of the body, which leads to a great incidence of *in vivo* click reactions in the blood in addition to ligations at the tumor after ^{99m}Tc-HYNIC-Polypeptide-PEG$_{11}$-Tz injection. In fact, the biodistribution data for 24 h accumulation showed that the uptake in the blood (1.60 ± 0.48 %IA/g) was even higher than that at the tumor (1.32 ± 0.14 %IA/g). The relatively lower activity level of blood and tumor in the accumulation interval of 72 h compared to 48 h was probably resulted from the slow isomerization conversion from TCO into less reactive cis-cyclooctene (CCO) due to the prolonged *in vivo* period of Cetuximab-TCO. Rossin et al. [24] investigated the deactivation mechanism of mAb-TCO *in vivo* and found that the TCO-CCO isomerization conversion via copper-containing proteins such as transcuprein, mouse serum albumin, and ceruloplasmin was the sole deactivation pathway of mAb-TCO in serum for a long time. CCO is of 5 orders of magnitude less reactive toward tetrazines than TCO.

According to the results of pretargeted biodistribution study, we chose the relatively most suitable accumulation interval (48 h) to compare the pretargeted Cetuximab-TCO/^{99m}Tc-HYNIC-PEG$_{11}$-Tz and Cetuximab-TCO/^{99m}Tc-HYNIC-Polypeptide-PEG$_{11}$-Tz biodistribution and SPECT imaging using subcutaneous HCT116 xenografts mice. The results demonstrated that the surplus unclicked ^{99m}Tc-HYNIC-PEG$_{11}$-Tz is cleared rapidly through the intestines into the faces and remained in it for a long time. The surplus unclicked ^{99m}Tc-HYNIC-Polypeptide-PEG$_{11}$-Tz is cleared completely through urinary system. The tumor/blood ratio was 1.61 ± 0.12 and 1.40 ± 0.31, respectively for pretargeted Cetuximab-TCO/^{99m}Tc-HYNIC-PEG$_{11}$-Tz and Cetuximab-TCO/^{99m}Tc-HYNIC-Polypeptide-PEG$_{11}$-Tz biodistribution. Both pretargeted imaging strategies delineated the HCT116 tumor clearly. However, pretargeted Cetuximab-TCO/^{99m}Tc-HYNIC-Polypeptide-PEG$_{11}$-Tz imaging avoided the retention of the surplus unclicked Tz-radioligand in faces, which favors to specific targeting imaging for CRC. Shi et al. [33] also once used a pretargeted strategy (Cetuximab-Tz or Panitumumab-Tz/Al[^{18}F]-NOTA-Reppe anhydride) for HCT116 tumor EGFR targeting imaging. In the study conducted by Shi et al., the tumor/blood ratio was 13.02 ± 0.64 and 10.15 ± 1.56, respectively for pretargeted Cetuximab-Tz and Panitumumab-Tz/Al[^{18}F]-NOTA-Reppe anhydride biodistribution. Both pretargeted imaging strategies delineated the HCT116 tumor clearly. However, due to the fact that Al[^{18}F]-NOTA-Reppe anhydride was excreted through hepatobiliary system and remained in faces for a long time, the authors were unable to resolve the problem that imaging agent remained in faces interfered with CRC imaging.

5. Conclusion

We successfully developed a novel pretargeted imaging strategy (Cetuximab-TCO/^{99m}Tc-HYNIC-Polypeptide-PEG$_{11}$-Tz) for imaging colorectal cancer since the surplus unclicked ^{99m}Tc-HYNIC-Polypeptide-PEG$_{11}$-Tz is cleared through urinary system and produces low abdominal uptake background, which further broadens the application scope of pretargeted imaging strategy.

List Of Abbreviations

ACN   Acetonitrile

CT   Computed Tomography

CPM   Counts per Minute

CRC   Colorectal cancer

CCO   Cis-cyclooctene

DMEM   Dulbecco's Modification of Eagle's Medium Dulbecco

DMF   N,N-Dimethylformamide

EGFR   Epidermal Growth Factor Receptor

FBS   Fetal Bovine Serum

HYNIC   6-hydrazinonicotinic Acid

IEDDA   Inverse Electron Demand [4+2] Diels-Alder cycloaddition

IFN-γ   Interferon-γ

keV   Kiloelectron Volt

LC-MS   Liquid Chromatography- Mass Spectrometry

MBq   Megabecquerel

MRI   Magnetic Resonance Imaging

NS   Normal Saline

PD-L1   Programmed Cell Death Ligand-1

PBS   Phosphate Buffer Saline

RCP   Radiochemical Purity

RP-HPLC Reversed-phase High-performance Liquid Chromatography

Rt   Retention Time

SEC-HPLC Size Exclusion Chromatography High-performance Liquid Chromatography

SPECT   Single Photon Emission Computed Tomography

Tz   1,2,4,5-terazine

TCO   Trans-cyslooctene

Tricine N-tris-hydroxymethyl-Methylglycine

^{18}F-FDG   2-deoxy-2-[^{18}F]fluoro-D-glucose

^{99m}Tc   Technetium-99m

%IA/g   Percentage of the Injected Activity Per Gram of Tissue Mass

Declarations

Acknowledgments

We want to thank for the technical supports from Prof. Yingjian Zhang and Dr. Jianping Zhang from Center for Biomedical Imaging, Fudan University, and Shanghai Engineering Research Center of Molecular Imaging Probes.

Authors' contributions

LQ, DFC and HCS designed the study and take responsibility for the integrity and accuracy of the data analysis. LQ, HT and DFC conceived and designed the experiments; LQ performed the main experiments and analysed the data; QYL, ZS, JZ and TTW helped do analysis and interpretation of data. LQ drafted the manuscript. DFC and HCS revised the manuscript. All authors contributed to this manuscript. All authors read and approved the final manuscript.

Funding

This study was funded by The National Nature Science Foundation of China (11875114, 81671735, and 81871407) and Open Large Infrastructure Research of Chinese Academy of Science.

Availability of data and materials

All data generated or analysed during this study are included in this published article and its supplementary information files.

Ethics approval and consent to participate

Animal care and all the procedures of animal experiments performed in this study were approved by the Animals Ethics Committee of Zhongshan Hospital, Fudan University.

Consent for publication

All authors agree to submit the article for publication.

Competing interests

The authors declare that they have no competing interests.

References

[1] Torre L A, Bray F, Siegel RL, Ferlay J, Lortet-Tieulent J, Jemal A. Global cancer statistics, 2012. CA Cancer J Clin. 2015;65(2):87-108.

[2] DeSantis CE, Lin CC, Mariotto AB, Siegel RL, Stein KD, Kramer JL, et al. Cancer treatment and survivorship statistics, 2014. CA Cancer J Clin. 2014;64(4):252-71.

[3] van Rijn JC, Reitsma JB, Stoker J, Bossuyt PM, van Deventer SJ, Dekker E, et al. Polyp miss rate determined by tandem colonoscopy: a systematic review. Am J Gastroenterol. 2006;101(2):343-50.

[4] Turker NS, Heidari P, Kucherlapati R, Kucherlapati M, Mahmood U. An EGFR targeted PET imaging probe for the detection of colonic adenocarcinomas in the setting of colitis. Theranostics. 2014;4(9):893-903.

[5] Liu J, Zuo X, Li C, Yu T, Gu X, Zhou C, et al. In vivo molecular imaging of epidermal growth factor receptor in patients with colorectal neoplasia using confocal laser endomicroscopy. Cancer Lett. 2013;330(2):200-7.

[6] Winkler AM, Rice PF, Weichsel J, Watson JM, Backer MV, Backer JM, et al. In vivo, dual-modality OCT/LIF imaging using a novel VEGF receptor-targeted NIR fluorescent probe in the AOM-treated mouse model. Mol Imaging Biol. 2011;13(6):1173-82.

[7] Hsiung PL, Hardy J, Friedland S, Soetikno R, Du CB, Wu AP, et al. Detection of colonic dysplasia in vivo using a targeted heptapeptide and confocal microendoscopy. Nat Med. 2008;14(4):454-8.

[8] Rusckowski M, Gupta S, Liu G, Dou S, Hnatowich DJ. Evidence of specificity of radiolabeled phage display peptides for the TAG-72 antigen. Cancer Biother Radiopharm. 2007;22(4):564-72.

[9] Yang M, Fan Q, Zhang R, Cheng K, Yan J, Pan D, et al. Dragon fruit-like biocage as an iron trapping nanoplatform for high efficiency targeted cancer multimodality imaging. Biomaterials. 2015;69:30-7.

[10] Yoon SM, Myung SJ, Kim IW, Do EJ, Ye BD, Ryu JH, et al. Application of near-infrared fluorescence imaging using a polymeric nanoparticle-based probe for the diagnosis and therapeutic monitoring of colon cancer. Dig Dis Sci. 2011;56(10):3005-13.

[11] Sartore-Bianchi A, Martini M, Molinari F, Veronese S, Nichelatti M, Artale S, et al. PIK3CA mutations in colorectal cancer are associated with clinical resistance to EGFR-targeted monoclonal antibodies. Cancer Res. 2009;69(5):1851-7.

[12] Aerts HJ, Dubois L, Perk L, Vermaelen P, van Dongen GA, Wouters BG, et al. Disparity between in vivo EGFR expression and 89Zr-labeled cetuximab uptake assessed with PET. J Nucl Med. 2009;50(1):123-31.

[13] Spiegelberg D, Mortensen AC, Selvaraju RK, Eriksson O, Stenerlow B, Nestor M. Molecular imaging of EGFR and CD44v6 for prediction and response monitoring of HSP90 inhibition in an in vivo squamous cell carcinoma model. Eur J Nucl Med Mol Imaging. 2016;43(5):974-82.

[14] Shih YH, Peng CL, Lee SY, Chiang PF, Yao CJ, Lin WJ, et al. 111In-cetuximab as a diagnostic agent by accessible epidermal growth factor (EGF) receptor targeting in human metastatic colorectal carcinoma. Oncotarget. 2015;6(18):16601-10.

[15] Guo Y, Parry JJ, Laforest R, Rogers BE, Anderson CJ. The role of p53 in combination radioimmunotherapy with 64Cu-DOTA-cetuximab and cisplatin in a mouse model of colorectal cancer. J Nucl Med. 2013;54(9):1621-9.

[16] Zeng D, Guo Y, White AG, Cai Z, Modi J, Ferdani R, et al. Comparison of conjugation strategies of cross-bridged macrocyclic chelators with cetuximab for copper-64 radiolabeling and PET imaging of EGFR in colorectal tumor-bearing mice. Mol Pharm. 2014;11(11):3980-7.

[17] Qiu L, Tan H, Lin Q, Si Z, Mao W, Wang T, et al. A Pretargeted Imaging Strategy for Immune Checkpoint Ligand PD-L1 Expression in Tumor Based on Bioorthogonal Diels-Alder Click Chemistry. Mol Imaging Biol. 2019;Nov 18 [Online ahead of print].

[18] Garcia MF, Gallazzi F, Junqueira MS, Fernandez M, Camacho X, Mororo JDS, et al. Synthesis of hydrophilic HYNIC-[1,2,4,5]tetrazine conjugates and their use in antibody pretargeting with (99m)Tc. Org Biomol Chem. 2018;16(29):5275-85.

[19] Rossin R, Verkerk PR, van den Bosch SM, Vulders RC, Verel I, Lub J, et al. In vivo chemistry for pretargeted tumor imaging in live mice. Angew Chem Int Ed Engl. 2010.49(19):3375-8.

[20] Rossin R, Lappchen T, van den Bosch SM, Laforest R, Robillard MS. Diels-Alder reaction for tumor pretargeting: in vivo chemistry can boost tumor radiation dose compared with directly labeled antibody. J Nucl Med. 2013;54(11):1989-95.

[21] Garcia MF, Zhang X, Shah M, Newton-Northup J, Cabral P, Cerecetto H, et al. (99m)Tc-bioorthogonal click chemistry reagent for in vivo pretargeted imaging. Bioorg Med Chem. 2016;24(6):1209-15.

[22] Zeglis BM, Sevak KK, Reiner T, Mohindra P, Carlin SD, Zanzonico P, et al. A pretargeted PET imaging strategy based on bioorthogonal Diels-Alder click chemistry. J Nucl Med. 2013;54(8):1389-96.

[23] Zeglis BM, Brand C, Abdel-Atti D, Carnazza KE, Cook BE, Carlin S, et al. Optimization of a Pretargeted Strategy for the PET Imaging of Colorectal Carcinoma via the Modulation of Radioligand Pharmacokinetics. Mol Pharm. 2015;12(10):3575-87.

[24] Rossin R, van den Bosch SM, Ten HW, Carvelli M, Versteegen RM, Lub J, et al. Highly reactive trans-cyclooctene tags with improved stability for Diels-Alder chemistry in living systems. Bioconjug Chem. 2013;24(7):1210-7.

[25] Nichols B, Qin Z, Yang J, Vera DR, Devaraj NK. 68Ga chelating bioorthogonal tetrazine polymers for the multistep labeling of cancer biomarkers. Chem Commun (Camb). 2014;50(40):5215-7.

[26] Devaraj NK, Thurber GM, Keliher EJ, Marinelli B, Weissleder R. Reactive polymer enables efficient in vivo bioorthogonal chemistry. Proc Natl Acad Sci U S A. 2012;109(13):4762-7.

[27] Garcia GE, Schweinsberg C, Maes V, Brans L, Blauenstein P, Tourwe DA, et al. Influence of the molecular charge on the biodistribution of bombesin analogues labeled with the [99mTc(CO)3]-core. Bioconjug Chem. 2008;19(12):2409-16.

[28] Tsiapa I, Loudos G, Varvarigou A, Fragogeorgi E, Psimadas D, Tsotakos T, et al. Biological evaluation of an ornithine-modified (99m)Tc-labeled RGD peptide as an angiogenesis imaging agent. Nucl Med Biol. 2013;40(2):262-72.

[29] Antunes P, Ginj M, Walter MA, Chen J, Reubi JC, Maecke HR. Influence of different spacers on the biological profile of a DOTA-somatostatin analogue. Bioconjug Chem. 2007;18(1):84-92.

[30] Meyer JP, Kozlowski P, Jackson J, Cunanan KM, Adumeau P, Dilling TR, et al. Exploring Structural Parameters for Pretargeting Radioligand Optimization. J Med Chem. 2017;60(19):8201-17.

[31] Janzer M, Larbig G, Kubelbeck A, Wischnjow A, Haberkorn U, Mier W. Drug Conjugation Affects Pharmacokinetics and Specificity of Kidney-Targeted Peptide Carriers. Bioconjug Chem. 2016;27(10):2441-9.

[32] Flook AM, Yang J, Miao Y. Substitution of the Lys linker with the beta-Ala linker dramatically decreased the renal uptake of 99mTc-labeled Arg-X-Asp-conjugated and X-Ala-Asp-conjugated alpha-melanocyte stimulating hormone peptides. J Med Chem. 2014;57(21):9010-8.

[33] Shi X, Gao K, Huang H, Gao R. Pretargeted Immuno-PET Based on Bioorthogonal Chemistry for Imaging EGFR Positive Colorectal Cancer. Bioconjug Chem. 2018;29(2):250-4.

Figures

HYNIC-PEG₁₁-Tz

HYNIC-Polypeptide-PEG₁₁-Tz
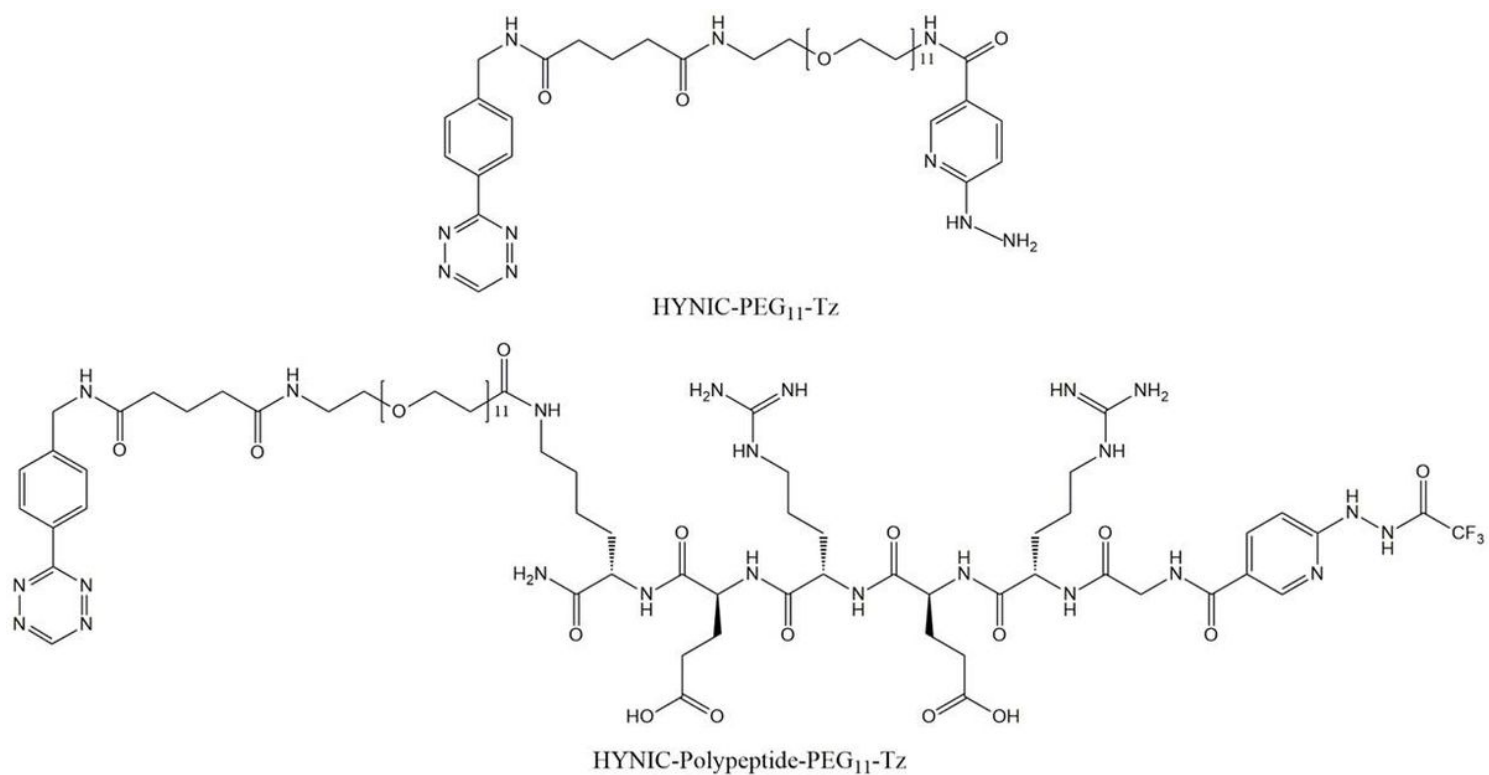
Figure 1

Chemical structures for HYNIC-PEG11-Tz and HYNIC-Polypeptide-PEG11-Tz.
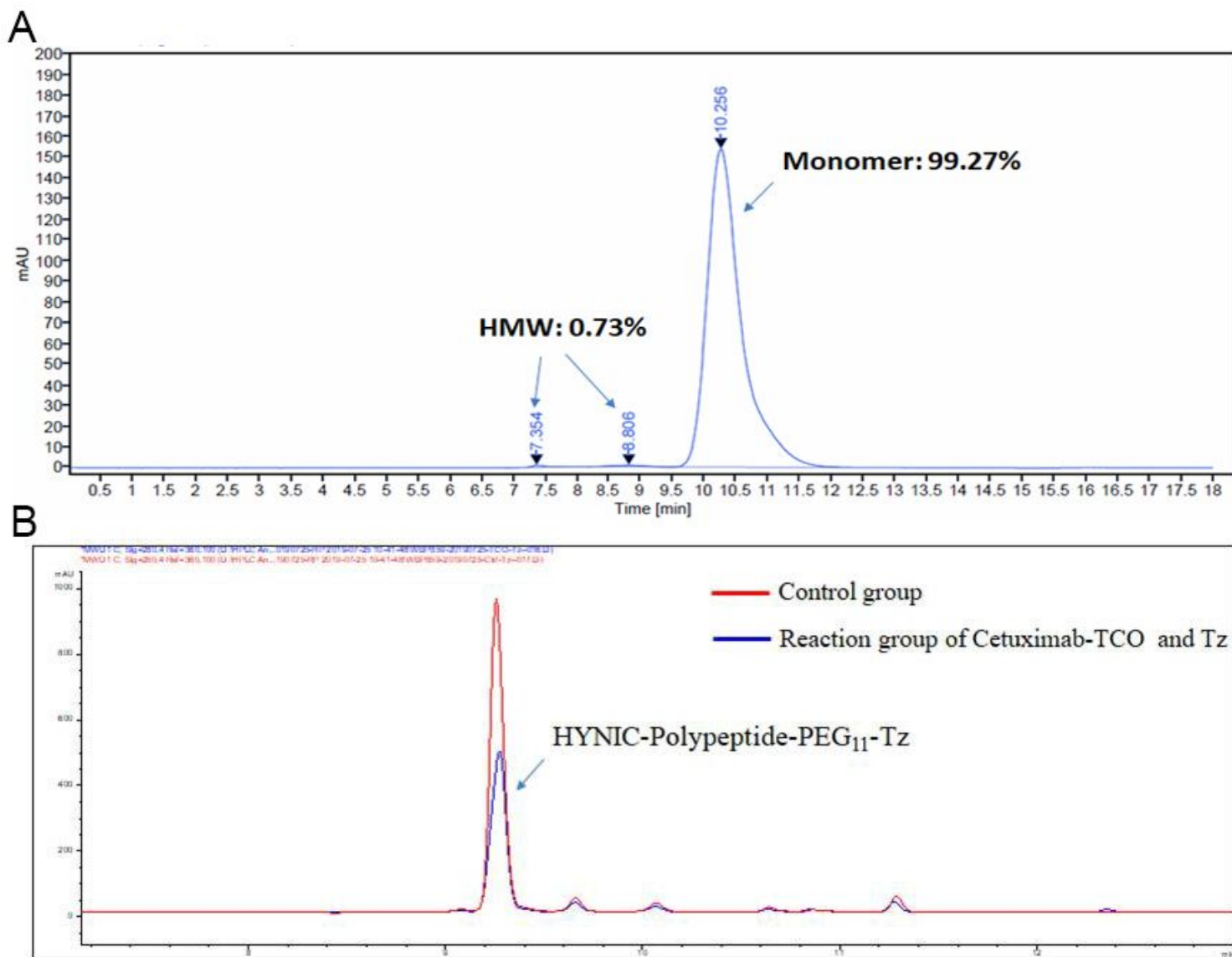
Figure 2

A. The aggregation level of this product is 0.73% and purity of the product is 99.27%. B. The peak (Rt = 9.3 min) at red and blue curve was the ultraviolet absorption peak of unclicked HYNIC-Polypeptide-PEG11-Tz at 280 nm in the control group and reaction group. The average reactive TCO moieties attached to each Cetuximab was 8.1.
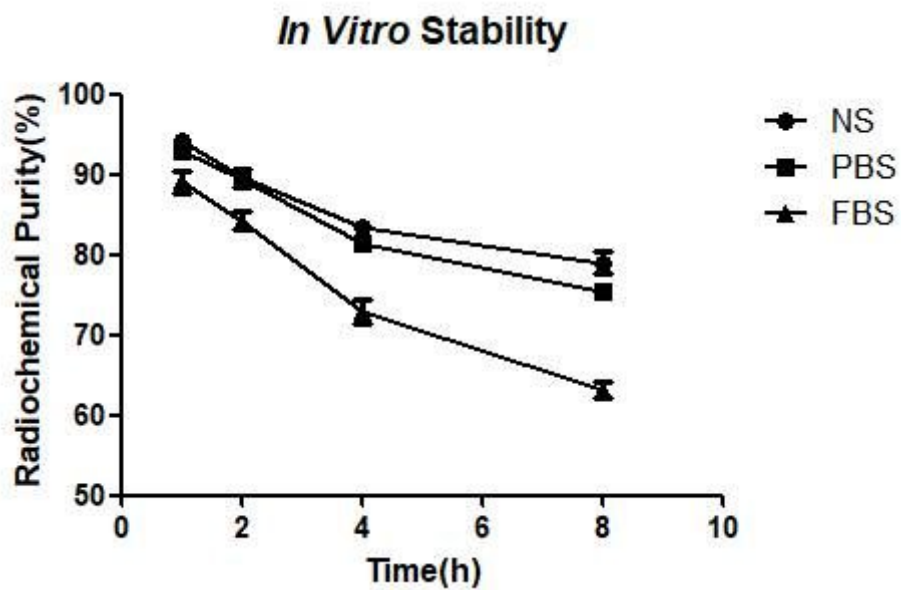
In Vitro Stability

Figure 3

In vitro stability of 99mTc-HYNIC-Polypeptide-PEG11-Tz.
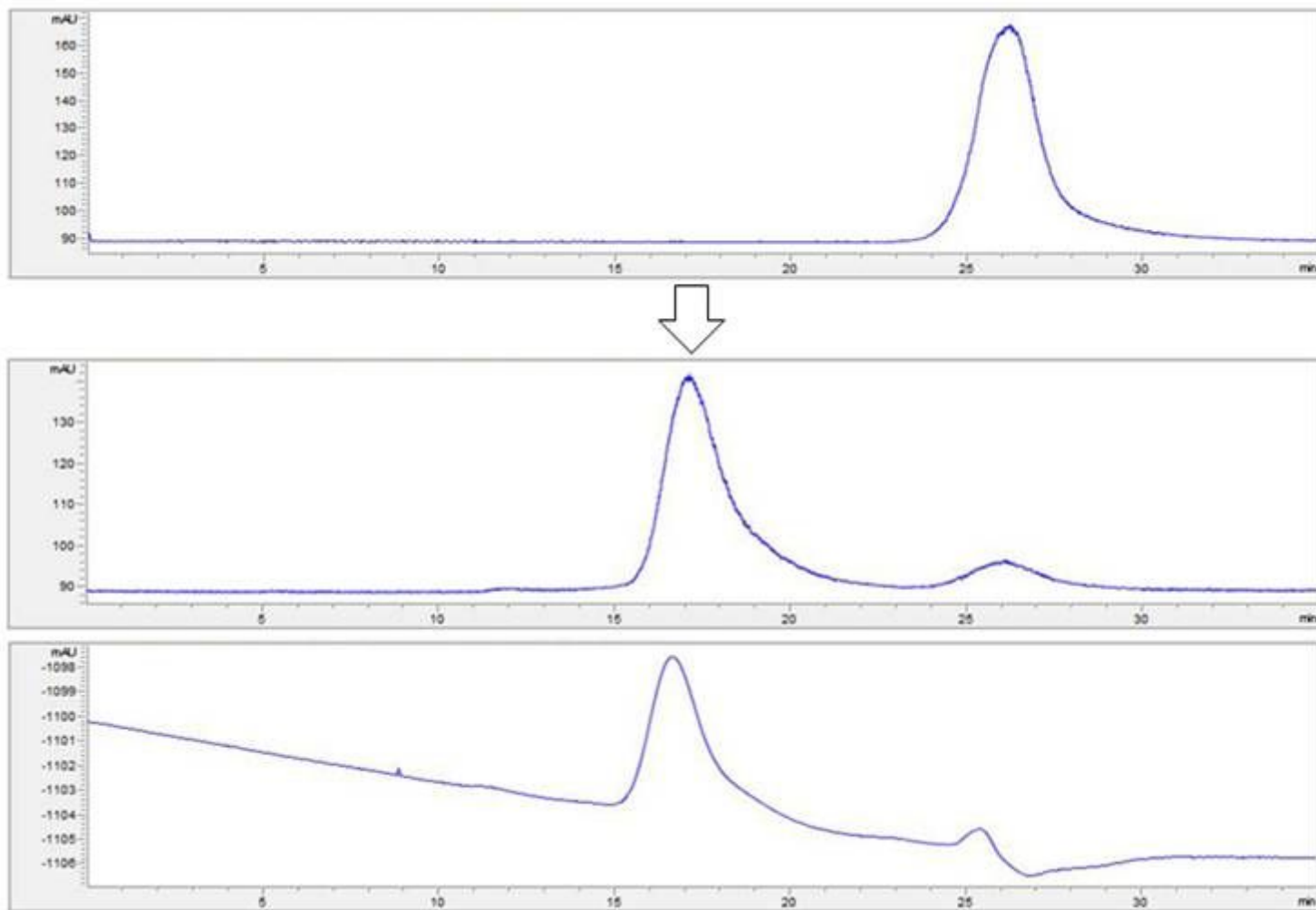
Figure 4

Top map: The radio-SEC-HPLC result for 99mTc-HYNIC-Polypeptide-PEG11-Tz alone. A peak was observed at the Rt = 26.14 min corresponding to the 99mTc-HYNIC-Polypeptide-PEG11-Tz. Middle map: The radio-SEC-HPLC result after incubation with the conjugation between 99mTc-HYNIC-Polypeptide-PEG11-Tz and Cetuximab-TCO in PBS for 30 min. The peak observed previously at Rt = 26.14 min had almost disappeared (The integral of the peak is 11.54%) concomitant with the appearance of a new peak at Rt = 16.05 min, indicating the formation of the "99mTc-HYNIC-Polypeptide-PEG11-Tz/TCO-Cetuximab" complex (The integral of the peak is 88.46%). Bottom map: The peak observed at Rt = 16.05 min and 26.14 min corresponds to the UV absorption peak at 280 nm for "99mTc-HYNIC-Polypeptide-PEG11-Tz/TCO-Cetuximab" complex and 99mTc-HYNIC-Polypeptide-PEG11-Tz, respectively.
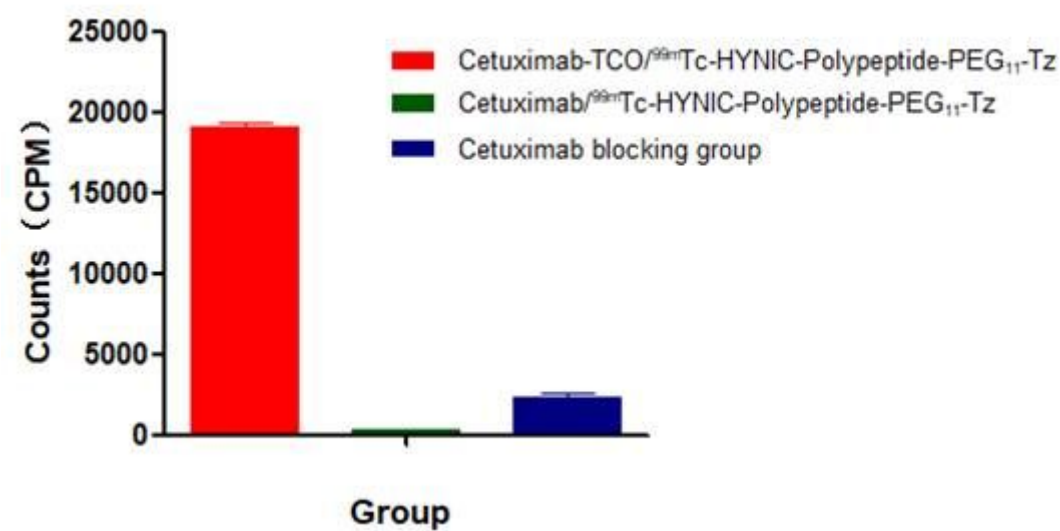
Figure 5

Pretargeted HCT116 cell immunoreactivity binding assay.

Figure 6

99mTc-HYNIC-Polypeptide-PEG11-Tz blood pharmacokinetics. The half-life of blood distribution is 15.72 ± 1.83 min.
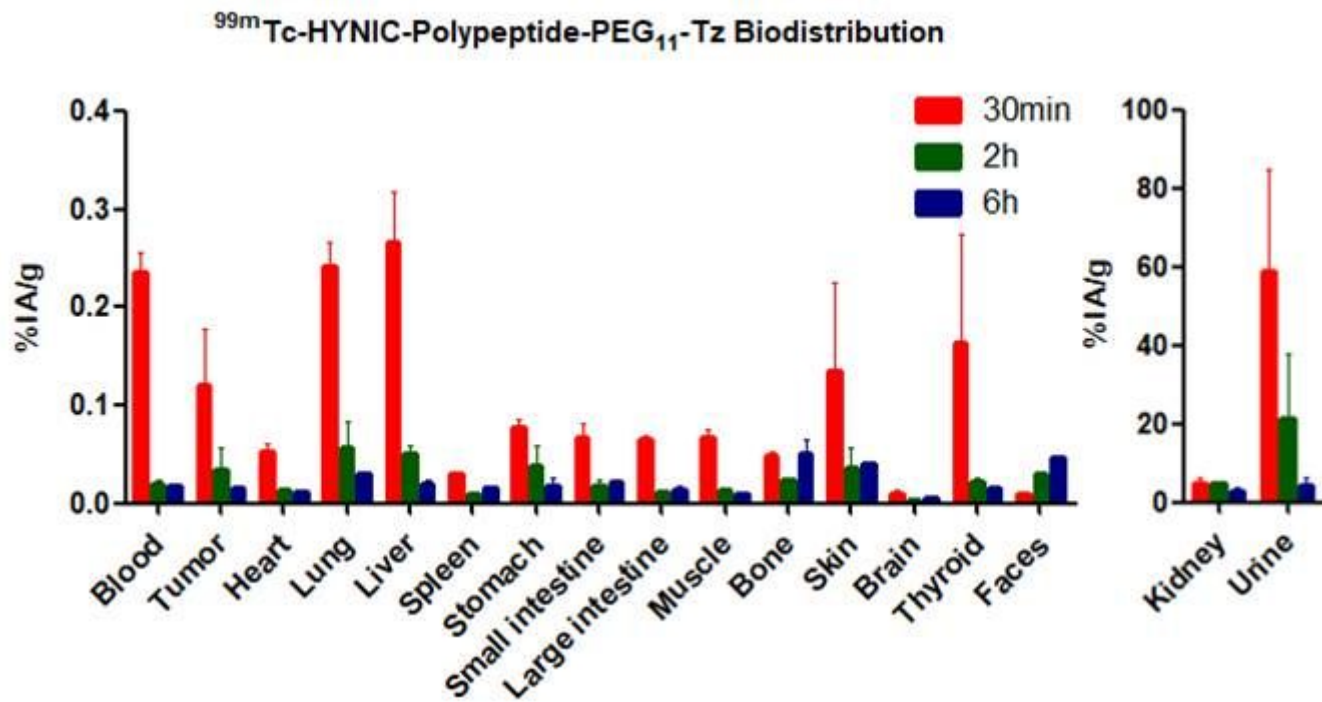
Figure 7

Biodistribution of 99mTc-HYNIC-Polypeptide-PEG11-Tz. Mice bearing HCT116 xenografts were administered 99mTc-HYNIC-Polypeptide-PEG11-Tz via tail vein injection. The mice were euthanized, and tissues of interest were harvested at 30 min, 2 h, and 6 h after the Tz-radioligand injection.
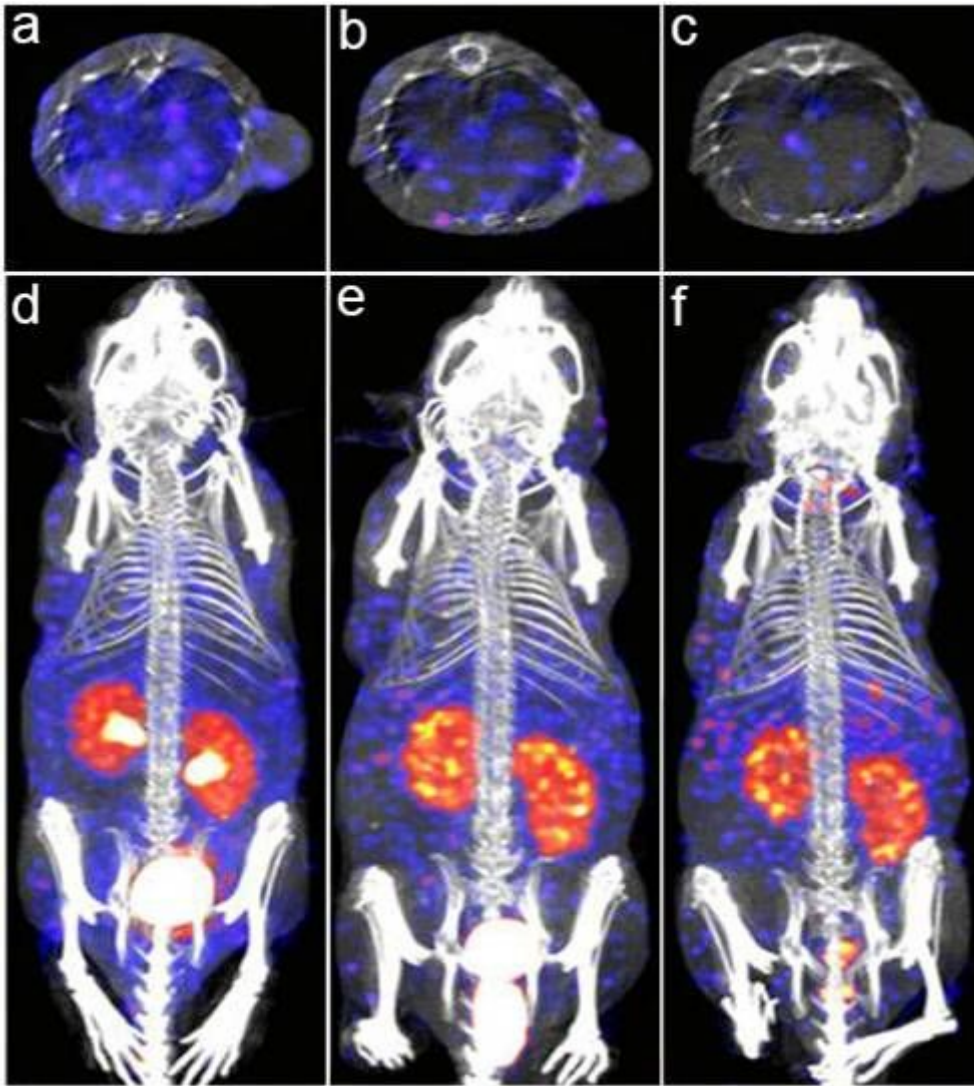
Figure 8

Small-animal SPECT/CT imaging of live mice bearing subcutaneous HCT116 xenografts at 30 min (a and d), 2 h (b and e), and 6 h (c and f) after 99mTc-HYNIC-Polypeptide-PEG11-Tz injection. a-c single transverse slices passing through the tumors in d-f (posterior projections).
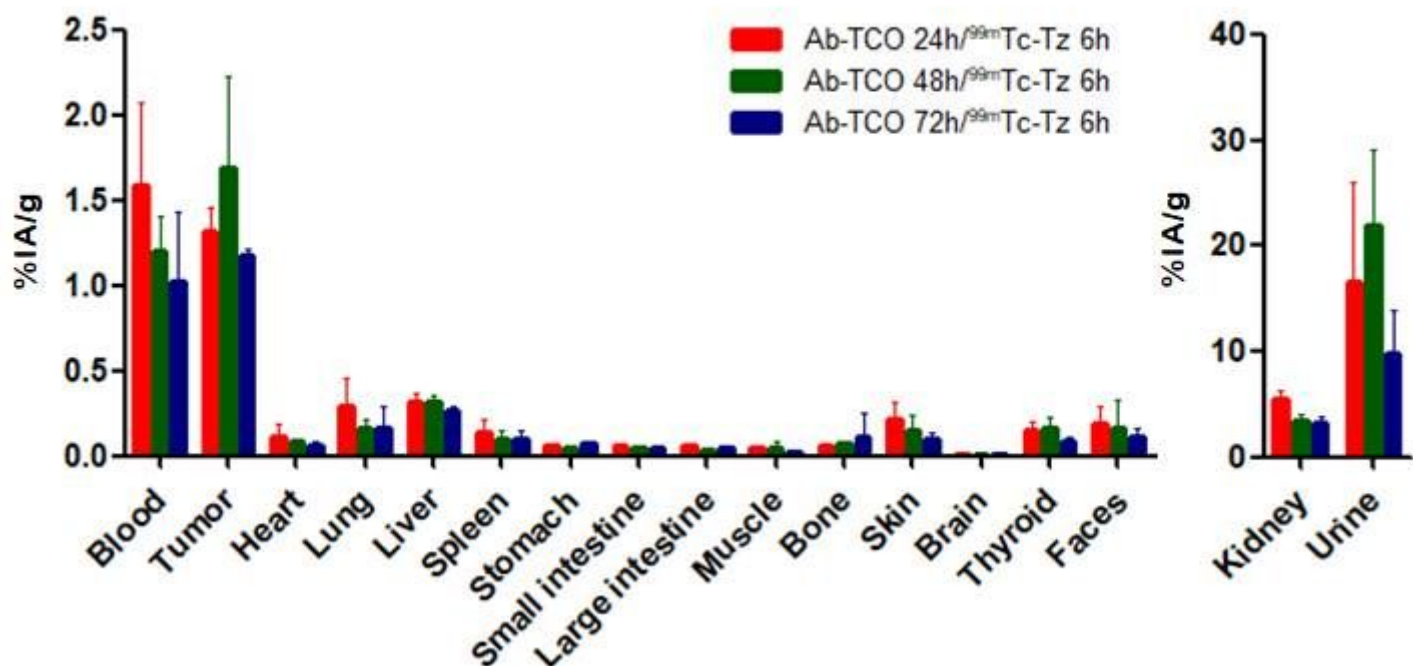
Figure 9

Biodistribution of live mice bearing subcutaneous HCT116 xenografts preinjected with Cetuximab-TCO followed 24 h, 48 h, and 72 h later by 99mTc-HYNIC-Polypeptide-PEG11-Tz. The animals were euthanized, and tissues of interest were harvested at 6 h after the Tz-radioligand injection.

Pretargeted Biodistribution Comparison
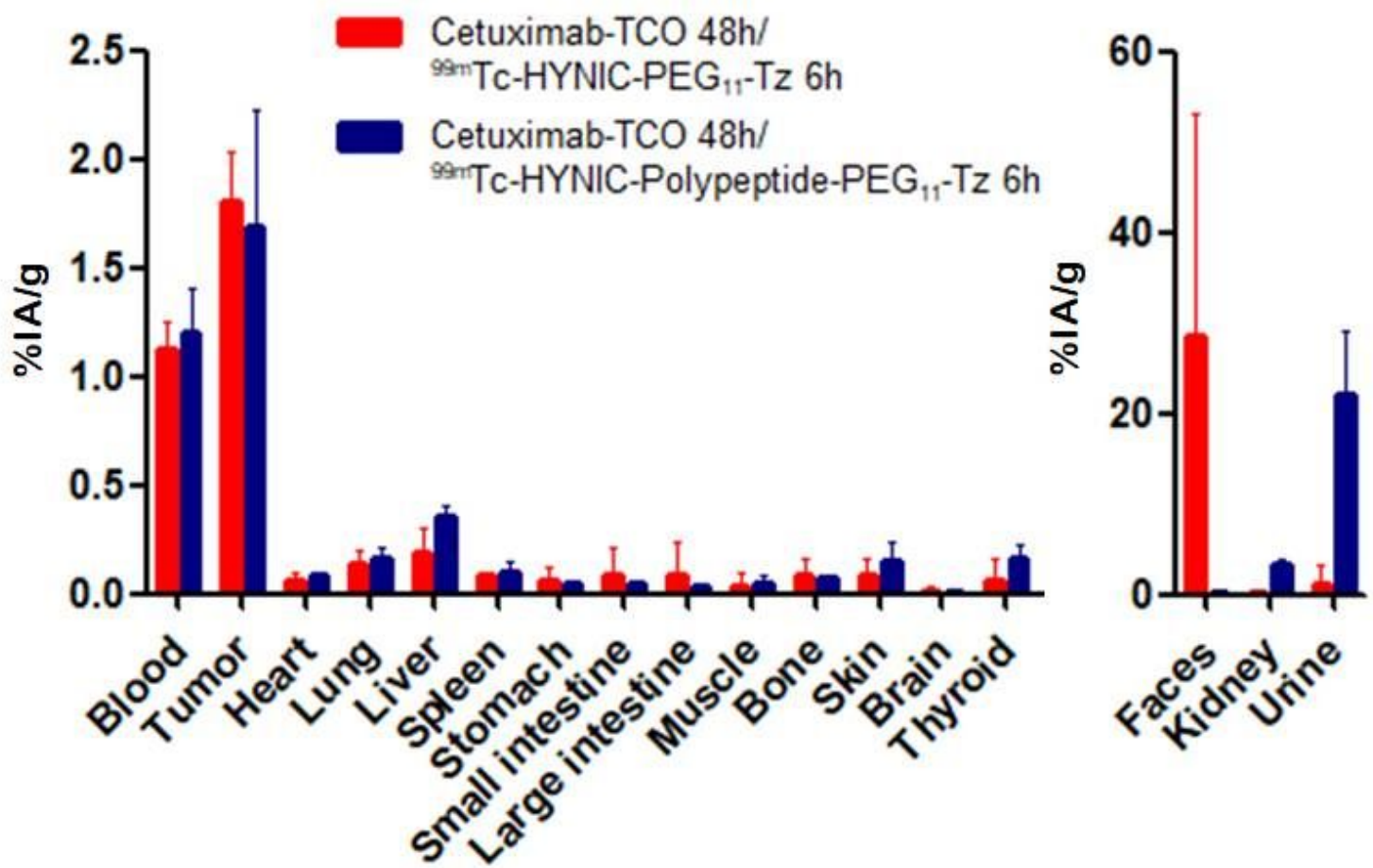
Figure 10

Biodistribution comparision of live mice bearing subcutaneous HCT116 xenografts preinjected with Cetuximab-TCO followed 48 h later by 99mTc-HYNIC-PEG11-Tz or 99mTc-HYNIC-Polypeptide-PEG11-Tz. The animals were euthanized, and tissues of interest were harvested at 6 h after 99mTc-HYNIC-PEG11-Tz or 99mTc-HYNIC-Polypeptide-PEG11-Tz injection.
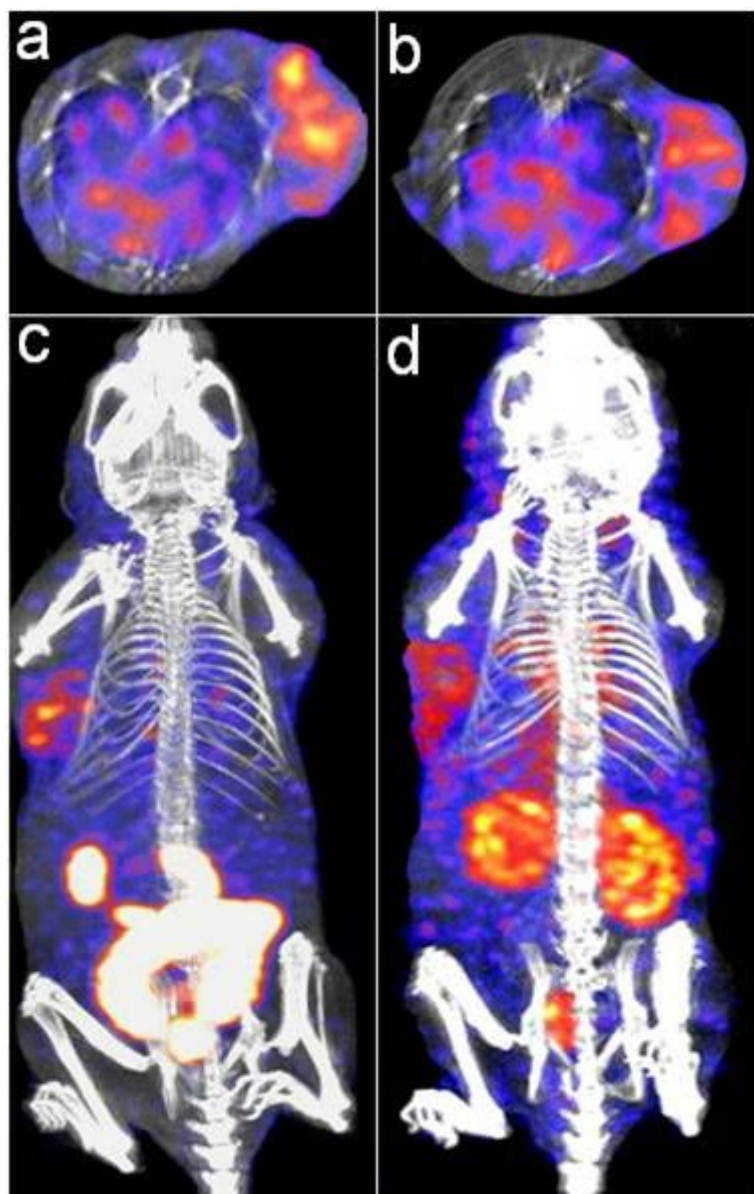
Figure 11

Pretargeted Cetuximab-TCO/99mTc-HYNIC-PEG11-Tz and Cetuximab-TCO/99mTc-HYNIC-Polypeptide-PEG11-Tz imaging comparison. Nude mice bearing subcutaneous HCT116 xenografts were administered Cetuximab-TCO 48 h prior to the injection of 99mTc-HYNIC-PEG11-Tz (a and c) or 99mTc-HYNIC-Polypeptide-PEG11-Tz (b and d) via the tail vein. The images were acquired at 6 h after 99mTc-HYNIC-PEG11-Tz or 99mTc-HYNIC-Polypeptide-PEG11-Tz injection. a-b single transverse slices passing through the tumors in c-d (posterior projections).